symmetry

MDPI

Article

Optimized Design for NB-LDPC-Coded High-Order CPM: Power and Iterative Efficiencies

Rui Xue [1], Tong Wang [1,*], Yanbo Sun [2] and Huaiyu Tang [3]

[1] College of Information and Communication Engineering, Harbin Engineering University, Harbin 150001, China; xuerui@hrbeu.edu.cn
[2] Southwest China Institute of Electronic Technology, Chengdu 610036, China; syb12345@hrbeu.edu.cn
[3] China Research Institute of Radiowave Propagation, Xinxiang 453000, China; tanghy@crirp.ac.cn
* Correspondence: wangtong736@hrbeu.edu.cn; Tel.: +86-188-4563-4648

Received: 17 July 2020; Accepted: 12 August 2020; Published: 13 August 2020

Abstract: In this paper, a non-binary low-density parity-check (NB-LDPC) coded high-order continuous phase modulation (CPM) system is designed and optimized to improve power and iterative efficiencies. Firstly, the minimum squared normalized Euclidean distance and the 99% double-sided power bandwidth are introduced to design a competitive CPM, improving its power efficiency under a given code rate and spectral efficiency. Secondly, a three-step method based on extrinsic information transfer (EXIT) and entropy theory is used to design NB-LDPC codes, which reduces the convergence threshold approximately 0.42 and 0.58 dB compared with the candidate schemes. Thirdly, an extrinsic information operation is proposed to address the positive feedback issue in iterative detection and decoding and the value of bit error rate (BER) can approximately be reduced by 5×10^{-3}. Finally, iteration optimization employing the EXIT chart and mutual information between demodulation and decoding is performed to achieve a suitable tradeoff for the communication reliability and iterative decoding delay. Simulation results show that the resulting scheme provides an approximately 3.95 dB coding gain compared to the uncoded CPM and achieves approximately 0.5 and 0.7 dB advantages compared with the candidate schemes. The resulting NB-LDPC-coded high-order CPM for a given code rate and spectral efficiency converges earlier into a turbo cliff region compared with other competitors and significantly improves power and iterative efficiencies.

Keywords: NB-LDPC code; CPM; iterative detection and decoding; iterative efficiency; power efficiency

1. Introduction

Continuous phase modulation (CPM) has the advantages of a continuous phase, constant envelope, high spectrum utilization, and excellent bandwidth efficiencies [1,2]. These characteristics are more notable for satellite systems with less power and fewer bandwidth resources, such as satellite navigation [3–5], satellite mesh networks [6,7], and satellite communication [8,9]. To further enhance the power and bandwidth efficiencies, coded CPM with symbol mapping using iterative decoding was presented. Considering the excellent properties of CPM and the serially concatenated principles [10,11], some particularly attractive solutions have become the focus of research, such as the convolutional [12,13], turbo [14–16], and low-density parity-check (LDPC) coded CPM [17–20].

As the serially concatenated CPM schemes in terms of convergence threshold are difficult to approach the Shannon limit, the non-binary (NB)-LDPC [21] code is considered the outer code, which has been the subject of numerous studies due to its excellent error correction capability. Unlike the traditional bit-interleaved coded modulation (BICM) systems, the interleaver of a high-order CPM works at the symbol level, which always yields a lower convergence threshold than the bit level [22].

The NB-LDPC code and high-order CPM have the same alphabet size, so the conversion information loss from bit to symbol caused by symbol mapping need not be considered [23].

To design and optimize coded CPM, previous works mainly focused on approaching the minimum signal-to-noise ratio (SNR) with a certain symmetry information rate (SIR) for a particular CPM with large block codes using large numbers of iterations [19]. This approach significantly limits the comprehensive analysis of a family of CPM schemes and is unsuitable for real-time applications due to excessive code length and decoding delay. Fortunately, A. G. Amat filled the gap and designed a suitable CPM using SIR among all CPM candidates [8], however, the SIR should be calculated for each CPM, which is a difficult task. Similarly, M. Foruhandeh used a systematic search procedure among all the candidates to identify the appropriate CPM scheme [20], achieving a targeted spectral efficiency and error rate, which results in considerable inconvenience in the CPM parameter design. Benaddi, T. derives an asymptotic analysis and optimization of coded CPM systems using both unstructured and protograph-based LDPC codes ensembles [24]. A practical system model with global interleaving is proposed for the optimization of degree distribution of the LDPC codes, which systematically solves the optimal system design of cascade irregular LDPC-CPM [25]. Zuohong Xu propose a two-stage decoding scheme mainly based on parity check matrix transform, which can efficiently improve the bit error rate performance [26]. All of the above schemes optimize the LDPC-CPM system to some extent, but they all adopt binary coding, the design and optimization of NB-LDPC-CPM system are still lacking. In summary, the major limitations of coded CPM optimization include CPM parameter design, decoding delay, the positive feedback problem in iterative decoding and the optimization of NB-LDPC.

This paper designed and optimized an NB-LDPC-coded high-order CPM to pursue high power efficiency and improve iterative efficiency under given spectral efficiency η and code rate R for practical considerations. Firstly, given the definite relationship between the SIR of CPM and minimum squared normalized Euclidean distance (MSNED), the MSNED and the 99% double-sided power bandwidth ($B_{99\%}$) are adopted to design a competitive CPM for a given R and η. Secondly, the code can be designed through a three-step method based on extrinsic information transfer (EXIT) and entropy theory when the CPM is determined. Thirdly, an extrinsic information operation is proposed in this paper to address the positive feedback problem in iterative detection and decoding, which problem may worsen bit error rate (BER) performance. Finally, an intensive study on proper iteration match between demodulation and decoding by the EXIT technique and mutual information was conducted to enhance systematic iterative efficiency and attain a suitable tradeoff between the communication reliability and iterative decoding delay.

The rest of this paper is organized as follows: Section 2 provides the principle block diagram of the proposed system, in which the modulation symbols are transmitted over the additive white Gaussian noise (AWGN) channel. A detailed analysis of the design process of a competitive CPM for particular R and η is shown in Section 3. Section 4 presents the analysis of the code design and the potential advantages of NB-LDPC-coded high-order CPM. The extrinsic information operation method, which curbs the positive feedback phenomenon in iterative decoding and detection, is outlined in Section 5. The iteration optimization of demodulation and decoding using the EXIT technique and mutual information is discussed in Section 6. Section 7 depicts the simulation results and feasibility. Finally, we conclude this paper in Section 8.

2. System Description

The principle block diagram of NB-LDPC-coded high-order CPM is shown in Figure 1. At the transmitter side, mapping and demapping from binary to Q-ary are required because the NB-LDPC encoder input $\mathbf{U}$ and output $\mathbf{C}$ are non-binary. Q is assumed to be equal to the cardinality M (M-ary, for example, quaternary and octal) of CPM. Then, the encoded sequence $\mathbf{C}$ is directly interleaved into $\mathbf{C}_I$ as the CPM modulator input. Finally, the complex signal vector $S(t, \boldsymbol{\alpha})$ produced by the M-ary CPM

modulator is divided as continuous phase encoder (CPE) and memoryless modulation (MM) [27] and transmitted over the AWGN channel.

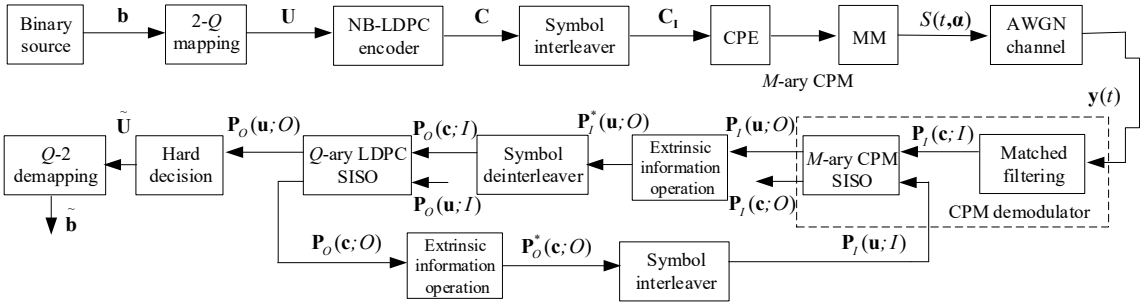

Figure 1. Non-binary low-density parity-check (NB-LDPC)-coded high-order continuous phase modulation (CPM) transmitter and receiver.

The demodulation and decoding of the receiver are accomplished through the iterations between CPM soft-input soft-output (SISO), which employs the maximum a posteriori (MAP)-like algorithm [28], and LDPC-SISO, which adopts the log-domain belief propagation (BP) with the fast Fourier transform algorithm [29,30]. SISO calculates the extrinsic a posterior probabilities (APPs) from the information and code symbol priori probabilities, and the decision device determines the symbol with a maximum APP in the last iteration.

3. Competitive CPM

3.1. SIR

The SIR is defined as the mutual information rate under the assumption that the input information is independent and identically distributed. To design an excellent coded CPM, the SIR is generally applied to design the best CPM scheme with the lowest E_s/N_0 required to achieve SIR. Given that CPM is a time invariant finite state machine (FSM) with complex signal outputs, the CPM system over an AWGN channel can be viewed as a finite state Markov channel (FSMC, Figure 2), and the SIR can be calculated using the algorithm developed in [31–34].

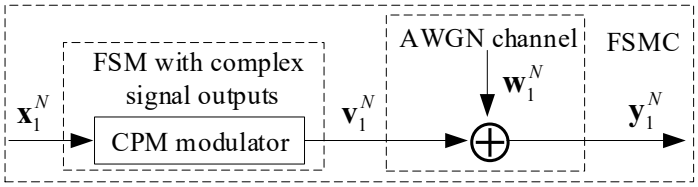

Figure 2. CPM model over an additive white Gaussian noise (AWGN) channel.

In Figure 2, $\mathbf{x}_1^N$ and $\mathbf{v}_1^N$ denote input information sequence and modulated sequence, respectively, and $\mathbf{y}_1^N$ is the output information sequence disturbed by AWGN sequence $\mathbf{w}_1^N$. Then, on the basis of the definition of channel capacity, the mutual information rate between $\mathbf{x}_1^N = (x_1, x_2, \ldots, x_N)$ and $\mathbf{y}_1^N = (y_1, y_2, \ldots, y_N)$ can be estimated as:

$$C = \lim_{N\to\infty} \frac{1}{N} I(\mathbf{x}_1^N, \mathbf{y}_1^N) = \lim_{N\to\infty} \frac{1}{N} \left[H(\mathbf{x}_1^N) - H(\mathbf{x}_1^N | \mathbf{y}_1^N) \right] = \log_2 M - \lim_{N\to\infty} \frac{1}{N} H(\mathbf{x}_1^N | \mathbf{y}_1^N) \quad (1)$$

where $H(\cdot)$ is an entropy function and $\mathbf{x}_1^N$ is independently and uniformly distributed. The expression $H(\mathbf{x}_1^N | \mathbf{y}_1^N)$ must also be calculated. $\mathbf{s}_0^N$ is defined as the state transition sequence of the CPM. $\mathbf{s}_0^N$ is a Markov random process and can only be related to $\mathbf{x}_1^N$; thus:

$$H(\mathbf{x}_1^N|\mathbf{y}_1^N) = H(\mathbf{s}_0^N|\mathbf{y}_1^N) = \sum_{i=1}^{N} H(s_i|s_{i-1}, \mathbf{y}_1^N) = -\sum_{i=1}^{N} p(s_i|s_{i-1}, \mathbf{y}_1^N) \log_2 p(s_i|s_{i-1}, \mathbf{y}_1^N). \quad (2)$$

In computing $p(s_i|s_{i-1}, \mathbf{y}_1^N)$, Bayes' rule transforms it to:

$$p(s_i|s_{i-1}, \mathbf{y}_1^N) = \frac{p(s_i, \mathbf{y}_1^N|s_{i-1})}{\sum_{s_i} p(s_i, \mathbf{y}_1^N|s_{i-1})}. \quad (3)$$

γ and β are introduced using the Bahl–Cocke–Jelinek–Raviv (BCJR)-like algorithm to estimate $p(s_i, \mathbf{y}_1^N|s_{i-1})$, and they are defined as follows [34]:

$$\gamma_i(s_{i-1}, s_i) = p(s_i, y_i|s_{i-1}) = p(y_i|s_{i-1}, s_i)p(s_i|s_{i-1}) = p(y_i|v_i)p(x_i) = \frac{1}{\sqrt{2\pi\sigma^2}} \exp\left(-\frac{\|y_i - v_i\|^2}{2\sigma^2}\right) p(x_i) \quad (4)$$

$$\beta_{i-1}(s_{i-1}) = p(\mathbf{y}_i^N|s_{i-1}) = \sum\nolimits_{s_i} p(s_i, \mathbf{y}_i^N|s_{i-1}) = \sum\nolimits_{s_i} p(\mathbf{y}_{i+1}^N|s_i)p(s_i, y_i|s_{i-1}) = \sum\nolimits_{s_i} \beta_i(s_i)\gamma_i(s_{i-1}, s_i) \quad (5)$$

where $\beta_N(s_N)$ is initialized as an equally likely state. Then, combining (4) and (5), $p(s_i|s_{i-1}, \mathbf{y}_1^N)$ is rewritten as:

$$p(s_i|s_{i-1}, \mathbf{y}_1^N) = \frac{\overline{\beta_i}(s_i)\gamma_i(s_{i-1}, s_i)}{\sum_{s_i} \overline{\beta_i}(s_i)\gamma_i(s_{i-1}, s_i)}, \quad (6)$$

with $\overline{\beta_i}(s_i) = \beta_i(s_i)/\sum_{s_i} \beta_i(s_i)$.

In Figure 3, the simulated SIR of CPM signals with 8M2 raised cosine (8M2RC) using various modulation index h ($h = p/q$, p, and q are the co-primes.) are shown, where 8M2RC denotes a particular CPM family with $M = 8$, memory length $L = 2$, and RC frequency pulse.

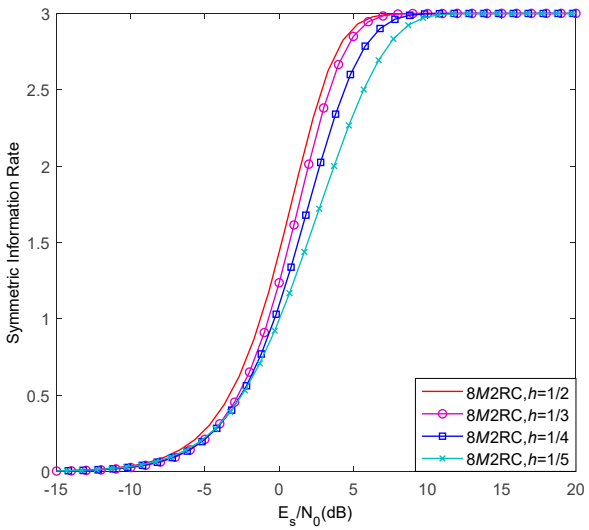

Figure 3. Symmetry information rate (SIR) of CPM with 8M2 raised cosine (8M2RC) using various h.

3.2. Design Criterion

The power and spectral efficiencies are influenced by the choice of M, h, pulse shape, memory, and code rate R. For example, a greater h, with the remaining parameters constant, typically results in increased power efficiency but at the expense of spectral efficiency. Similarly, increasing M will increase the spectral efficiency and decrease the power efficiency. Lowering R alone can increase the coding gain but decrease the spectral efficiency. Thus, the combination of code and modulation parameters for coded CPM must be chosen carefully based on these constraints.

In practical applications, CPM demodulator complexity must be considered, which is dependent on the total number of matched filters and trellis states. The complexity could be represented as qM^L matched filters followed by the CPM-SISO detector with the trellis of PM^{L-1} states. All the CPM schemes subject to the constraints $q \leq 5$, $L < 3$ and $M \leq 8$ are analyzed in this paper to reduce the implementation complexity.

In Table 1, the MSNED $d^2_{\min}$ and $B_{99\%}T_b$ of all candidate CPM schemes with RC and rectangle (REC) frequency pulses under the constraints (i.e., $q \leq 5$, $L < 3$, $M \leq 8$, and $h < 1$) are calculated, where T_b is the bit period, and MSNED can be expressed by [10]:

$$d^2_{\min} = \log_2 M \min_i \left\{ \frac{1}{T_s} \int_0^{NT_s} [1 - \cos \phi(t, \boldsymbol{\chi}_i)] dt \right\} \tag{7}$$

with

$$\phi(t, \boldsymbol{\chi}_i) = 2\pi h \sum_j \chi_{i,j} \int_{-\infty}^{t} g(\tau) d\tau, \boldsymbol{\chi}_i = \boldsymbol{\alpha} - \overline{\boldsymbol{\alpha}} \tag{8}$$

where NT_s denotes observation symbol intervals and $\boldsymbol{\chi}_i$ is the difference between the transmitted sequence $\boldsymbol{\alpha}$ and the received sequence $\overline{\boldsymbol{\alpha}}$. The values of $\chi_{i,j}$ are obtained from $\{0, \pm 2, \pm 4, \ldots, \pm 2(M-1)\}$. $B_{99\%}$ can be computed indirectly by:

$$0.99 = \int_{-B_{99\%}/2}^{B_{99\%}/2} G(f) df \tag{9}$$

where $G(f)$ is the normalized power spectrum density of CPM and is defined as:

$$\begin{aligned} G(f) = 2\Bigg\{ & \int_0^{LT} \mathfrak{R}(\tau) \cos 2\pi f \tau d\tau + \frac{1 - \psi(jh) \cos 2\pi f T}{1 + \psi^2(jh) - 2\psi(jh) \cos 2\pi f T} \times \int_{LT}^{(L+1)T} \mathfrak{R}(\tau) \cos 2\pi f \tau d\tau \\ & - \frac{\psi(jh) \sin 2\pi f T}{1 + \psi^2(jh) - 2\psi(jh) \cos 2\pi f T} \times \int_{LT}^{(L+1)T} \mathfrak{R}(\tau) \sin 2\pi f \tau d\tau \Bigg\} \end{aligned} \tag{10}$$

With:

$$\psi(jh) = \sin M\pi h / M \sin \pi h \tag{11}$$

where $\mathfrak{R}(\tau)$ denotes the autocorrelation function of CPM:

$$\mathfrak{R}(\tau) = \frac{1}{T} \int_0^T \prod_{k=1-L}^{\lfloor \tau/T \rfloor} \frac{1}{M} \frac{\sin 2\pi h M [q(t + \tau - kT) - q(t - kT)]}{\sin 2\pi h [q(t + \tau - kT) - q(t - kT)]} dt \tag{12}$$

where $\lfloor \cdot \rfloor$ is a floor rounding operator.

Table 1. $d^2_{\min}$ and $B_{99\%}T_b$ of all candidate CPM schemes subject to constraints $q \leq 5$, $L < 3$, $M < 8$, and $h < 1$.

h	**4*M*1REC**	**4*M*1RC**	**8*M*1REC**	**8*M*1RC**
1/5	$B_{99\%}T_b = 0.65, d^2_{\min} = 0.97$	$B_{99\%}T_b = 1.06, d^2_{\min} = 1.13$	$B_{99\%}T_b = 0.76, d^2_{\min} = 1.46$	$B_{99\%}T_b = 1.15, d^2_{\min} = 1.69$
1/4	$B_{99\%}T_b = 0.81, d^2_{\min} = 1.45$	$B_{99\%}T_b = 1.25, d^2_{\min} = 1.66$	$B_{99\%}T_b = 0.91, d^2_{\min} = 2.18$	$B_{99\%}T_b = 1.36, d^2_{\min} = 2.49$
1/3	$B_{99\%}T_b = 0.99, d^2_{\min} = 2.35$	$B_{99\%}T_b = 1.49, d^2_{\min} = 2.25$	$B_{99\%}T_b = 1.12, d^2_{\min} = 3.50$	$B_{99\%}T_b = 1.78, d^2_{\min} = 3.33$
2/5	$B_{99\%}T_b = 1.09, d^2_{\min} = 3.06$	$B_{99\%}T_b = 1.67, d^2_{\min} = 2.40$	$B_{99\%}T_b = 1.31, d^2_{\min} = 4.60$	$B_{99\%}T_b = 2.09, d^2_{\min} = 3.60$
1/2	$B_{99\%}T_b = 1.28, d^2_{\min} = 4.00$	$B_{99\%}T_b = 1.95, d^2_{\min} = 2.24$	$B_{99\%}T_b = 1.54, d^2_{\min} = 6.00$	$B_{99\%}T_b = 2.52, d^2_{\min} = 3.36$
3/5	$B_{99\%}T_b = 1.49, d^2_{\min} = 3.50$	$B_{99\%}T_b = 2.26, d^2_{\min} = 2.40$	$B_{99\%}T_b = 1.79, d^2_{\min} = 5.24$	$B_{99\%}T_b = 2.96, d^2_{\min} = 3.60$
2/3	$B_{99\%}T_b = 1.57, d^2_{\min} = 3.57$	$B_{99\%}T_b = 2.49, d^2_{\min} = 2.60$	$B_{99\%}T_b = 1.96, d^2_{\min} = 5.37$	$B_{99\%}T_b = 3.31, d^2_{\min} = 3.90$
3/4	$B_{99\%}T_b = 1.71, d^2_{\min} = 3.72$	$B_{99\%}T_b = 2.81, d^2_{\min} = 2.90$	$B_{99\%}T_b = 2.16, d^2_{\min} = 5.58$	$B_{99\%}T_b = 3.68, d^2_{\min} = 4.15$
4/5	$B_{99\%}T_b = 1.83, d^2_{\min} = 3.84$	$B_{99\%}T_b = 2.98, d^2_{\min} = 3.37$	$B_{99\%}T_b = 2.28, d^2_{\min} = 5.72$	$B_{99\%}T_b = 3.89, d^2_{\min} = 4.28$
h	**4*M*2REC**	**4*M*2RC**	**8*M*2REC**	**8*M*2RC**
1/5	$B_{99\%}T_b = 0.44, d^2_{\min} = 0.64$	$B_{99\%}T_b = 0.56, d^2_{\min} = 0.88$	$B_{99\%}T_b = 0.57, d^2_{\min} = 0.96$	$B_{99\%}T_b = 0.63, d^2_{\min} = 1.32$
1/4	$B_{99\%}T_b = 0.53, d^2_{\min} = 0.98$	$B_{99\%}T_b = 0.64, d^2_{\min} = 1.33$	$B_{99\%}T_b = 0.68, d^2_{\min} = 1.48$	$B_{99\%}T_b = 0.75, d^2_{\min} = 1.99$
1/3	$B_{99\%}T_b = 0.69, d^2_{\min} = 1.69$	$B_{99\%}T_b = 0.79, d^2_{\min} = 2.16$	$B_{99\%}T_b = 0.87, d^2_{\min} = 2.52$	$B_{99\%}T_b = 0.95, d^2_{\min} = 3.30$
2/5	$B_{99\%}T_b = 0.81, d^2_{\min} = 2.35$	$B_{99\%}T_b = 0.91, d^2_{\min} = 2.91$	$B_{99\%}T_b = 1.02, d^2_{\min} = 3.53$	$B_{99\%}T_b = 1.11, d^2_{\min} = 4.36$
1/2	$B_{99\%}T_b = 0.99, d^2_{\min} = 3.45$	$B_{99\%}T_b = 1.06, d^2_{\min} = 3.71$	$B_{99\%}T_b = 1.26, d^2_{\min} = 5.18$	$B_{99\%}T_b = 1.32, d^2_{\min} = 5.56$
3/5	$B_{99\%}T_b = 1.15, d^2_{\min} = 4.60$	$B_{99\%}T_b = 1.22, d^2_{\min} = 3.75$	$B_{99\%}T_b = 1.49, d^2_{\min} = 6.31$	$B_{99\%}T_b = 1.58, d^2_{\min} = 5.63$
2/3	$B_{99\%}T_b = 1.26, d^2_{\min} = 4.00$	$B_{99\%}T_b = 1.33, d^2_{\min} = 3.47$	$B_{99\%}T_b = 1.64, d^2_{\min} = 6.01$	$B_{99\%}T_b = 1.74, d^2_{\min} = 5.20$
3/4	$B_{99\%}T_b = 1.39, d^2_{\min} = 4.19$	$B_{99\%}T_b = 1.45, d^2_{\min} = 3.71$	$B_{99\%}T_b = 1.84, d^2_{\min} = 6.28$	$B_{99\%}T_b = 1.93, d^2_{\min} = 5.56$
4/5	$B_{99\%}T_b = 1.47, d^2_{\min} = 4.88$	$B_{99\%}T_b = 1.51, d^2_{\min} = 4.11$	$B_{99\%}T_b = 1.95, d^2_{\min} = 6.00$	$B_{99\%}T_b = 2.05, d^2_{\min} = 6.16$

A definite relationship between SIR and MSNED can be presented in Table 1 and Figure 3. The SIR curve of CPM with the highest MSNED converges earliest and corresponds to the lowest bound denoted as the minimum E_s/N_0, which can be traced back from the SIR curve by the $R \log_2 M$. For instance, the SIR of 8*M*2RC using h = 1/2 converges earliest, followed by h = 1/3, 1/4, and 1/5, because the 8*M*2RC using h = 1/2 has the highest $d^2_{\min}$ of 5.56, followed by h = 1/3, 1/4, and 1/5. The computational complexity of MSNED is significantly lower than SIR, which provides convenience in designing a competitive CPM. Thus, we used $B_{99\%}T_b$ and MSNED instead of SIR curves to design the suitable scheme from all candidate CPM signals under a given code rate R and spectral efficiency η.

The relationship of the coded modulation systems among M, R, $B_{99\%}$, T_s, and η is defined as:

$$\eta = \frac{R \log_2 M}{B_{99\%}T_s} = \frac{R}{B_{99\%}T_b} \tag{13}$$

For the given η and R, the $B_{99\%}T_b$ can be attained using (13). The competitive CPM scheme can be determined by the highest $d^2_{\min}$ among these candidate CPM signals with corresponding $B_{99\%}T_b$. For example, η and R are 0.5 bit/s/Hz and 2/3, respectively, $B_{99\%}T_b$ is approximately computed as 1.33 using (13). Table 1 shows that the 8*M*2RC with h = 1/2, 8*M*1REC with h = 2/5, and 4*M*2RC with h = 2/3 can approximately meet the constraint of $B_{99\%}T_b$, and the $d^2_{\min}$ of the three schemes are 5.56, 4.60, and 3.47, respectively. Consequently, 8*M*2RC with h = 1/2 is preferred as the competitive CPM scheme due to its highest $d^2_{\min}$ relative to other candidates. The competing CPM schemes for other η and R can also be selected according to (13) and Table 1.

4. Code Design and Advantages

4.1. EXIT Technique

The EXIT chart [35] is a powerful technique for predicting the iterative detection convergence using SISO modules. Similar to the density evolution, this technique assumes extrinsic information in SISO decoders as independent Gaussian random variables. Figure 4 depicts the extrinsic information interaction between two SISO decoders of NB-LDPC-coded high-order CPM. CPM-SISO has two inputs of the prior information from the interleaver and the inner codeword information from matched filters. As the inner codeword information is connected to E_b/N_0, the average mutual information of the CPM-SISO output can be treated as a function of the average mutual information of the input I_A^{CPM} and E_b/N_0, given by:

$$I_E^{CPM} = T_{CPM-SISO}(I_A^{CPM}, E_b/N_0) \tag{14}$$

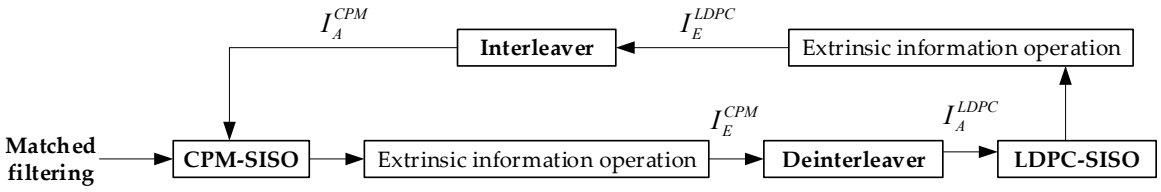

Figure 4. Serially iterative decoder of NB-LDPC-coded high-order CPM.

The average mutual information of the LDPC-SISO output I_E^{LDPC} is only related to the average mutual information of the input I_A^{LDPC}, resulting in:

$$I_E^{LDPC} = T_{LDPC-SISO}(I_A^{LDPC}) \tag{15}$$

where functions $T_{CPM-SISO}(\cdot)$ and $T_{LDPC-SISO}(\cdot)$ are defined as the EXIT characteristics of CPM-SISO and LDPC-SISO, respectively.

4.2. NB-LDPC Code Design

A three-step method is used in this paper to design the following NB-LDPC codes.

(1) Optimization of degree distribution based on binary parity-matrix using the EXIT technique. The NB-LDPC code has the same Tanner graph and degree distribution property as its corresponding binary representation, except for non-zero values; thus, the EXIT chart was used to explore a binary sparse matrix with acceptable degree distribution. Figure 5 provides the EXIT characteristics of different variable node (VN) and check node (CN) degrees.

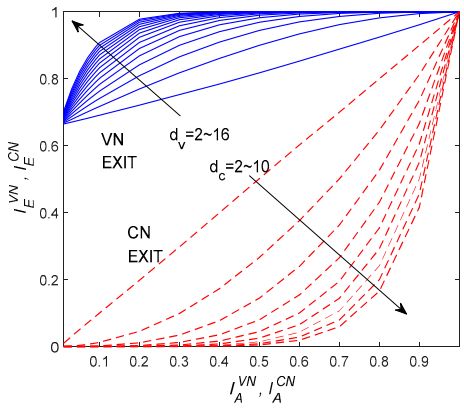

Figure 5. Variable node (VN) and check node (CN) extrinsic information transfer (EXIT) curves with various degrees under R = 2/3 and $\mathrm{E_b}/\mathrm{N_0} = 1$dB.

To design a suitable degree profile consisting of VN and CN degree distributions, a general approach described in [36] was used by fixing the CN degree distribution, and then changing the VN degree distribution to search the lowest convergence threshold. The area between the VN EXIT curve and the inverse CN EXIT curve is the smallest without intersections. The degree distribution corresponding to the lowest convergence threshold is optimal. This systematic search procedure can be performed as follows:

$$I_E^{VN} = \sum_{i=2}^{d_v} \lambda_i J\left(\sqrt{(i-1)\left[J^{-1}(I_A^{VN})\right]^2 + 8R\frac{\mathrm{E_b}}{\mathrm{N_0}}}\right) \tag{16}$$

$$I_E^{CN} = 1 - \sum_{i=2}^{d_c} \rho_i J(\sqrt{i-1} \times J^{-1}(1 - I_A^{CN})) \tag{17}$$

where d_v and d_c are the maximum VN and CN degrees, respectively; λ_i and ρ_i express the fractions of edges connecting to VNs and CNs of degree i while satisfying $\sum_{i=2}^{d_v} \lambda_i = 1$ and $\sum_{i=2}^{d_c} \rho_i = 1$, respectively. The function $J(\cdot)$ and its inverse function $J^{-1}(\cdot)$ are defined in [33]. Equations (16) and (17) are linear weighted sums of VN and CN EXIT curves of the given R and $\mathrm{E_b}/\mathrm{N_0}$, respectively. The entire process of searching for a suitable degree distribution must be subjected to the constraint, that is:

$$R = 1 - \frac{\sum_{i=2}^{d_c} \frac{\rho_i}{i}}{\sum_{i=2}^{d_v} \frac{\lambda_i}{i}} = 1 - \frac{\int_0^1 \rho(x)dx}{\int_0^1 \lambda(x)dx} \tag{18}$$

with $\rho(x) = \sum_{i=2}^{d_c} \rho_i x^{i-1}$ and $\lambda(x) = \sum_{i=2}^{d_v} \lambda_i x^{i-1}$.

(2) Construction of a parity-check matrix with a large girth. After determining the degree distribution, the positions of non-zero elements in binary parity-check matrix $\mathbf{H}_b$ must be ascertained. A girth optimization tool, called progressive edge growth [37], is adopted to avoid small circles and achieve good girth properties when using the BP-like algorithm on the Tanner graph.

(3) Choice of non-zero elements over GF(Q). Generally, this step can be performed by substituting the "1" elements of $\mathbf{H}_b$ with random non-zero elements over GF(Q), which can provide acceptable performance in most cases. Entropy theory, which is the appropriate measure for uncertainty, is introduced to improve the uncertainty or randomness of cycles located at the Tanner graph, which helps obtain a low error rate. First, the cycle-searching algorithm proposed in [38] is applied to search all small circles of $\mathbf{H}_b$ with lengths $l = 4, 6$, and even 8 if necessary, and record the corresponding positions of non-zero elements in each circle. Next, a general method for constructing the NB-LDPC code is employed to randomly replace all the "1" elements of $\mathbf{H}_b$ with non-zero elements of GF(Q). Eventually, the entropy of each previously recorded circle is calculated and maximized when each element takes various non-zero values over GF(Q), that is:

$$E_n = -\sum_{i=1}^{Q-1} Pr_i \log_2 Pr_i \tag{19}$$

where $Pr_i = n_i/l$ and n_i denote the appearance times of i in each circle with $i \in [1, 2, \cdots, Q-1]$.

In the case of $R = 2/3$ and $\eta = 0.5$ bit/s/Hz, based on (14) and (15), the EXIT chart of the resulting scheme using 8M2RC concatenated with designed NB-LDPC code was drawn in Figure 6, where the convergence threshold is 0.81 dB.

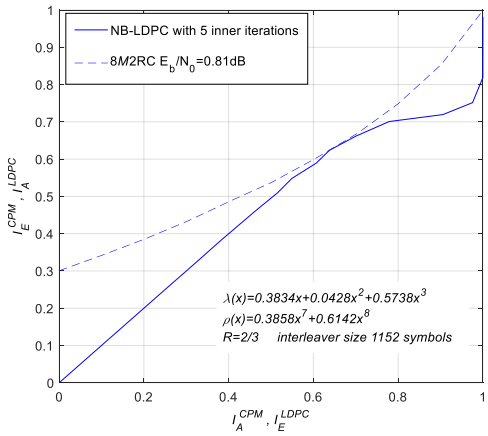

Figure 6. EXIT chart of the optimized NB-LDPC-coded high-order CPM system with 8M2RC under five inner iterations.

4.3. Additional Advantages

The investigation into NB-LDPC-coded high-order CPM is particularly significant for coded modulation systems. In addition to the excellent properties in terms of continuous phase, rapidly decaying spectrum side lobes, and constant envelope, this scheme has the following additional advantages:

(1) Each edge of the binary LDPC code in the Tanner graph carries bit messages, but the NB-LDPC code carries Q-ary symbol messages, thus, short girths are avoided in the Tanner graph. This reduces the influence of short girths and stopping set on decoding convergence. Therefore, the BP algorithm becomes closer to the maximum likelihood decoding algorithm. The NB-LDPC code, as an outer code in coded modulation systems, provides an alternative solution in enhancing BER performance in practical applications.

(2) In comparison with the traditional BICM, the interleaver of the NB-LDPC-coded high-order CPM works at the symbol level, which always yields a lower convergence threshold than bit level. This advantage is rather significant in a serial concatenation [22].

(3) As the NB-LDPC code and CPM select the uniform M-ary in the investigated systems, the symbol mapping issue that is likely to result in conversion information loss from bit to symbol may be ignored. This phenomenon usually occurs in the case of $M > q$. Thus, more possible input code symbols exist between the current and next phase states in the trellis diagrams. For an example of the CPM scheme with 8M2RC using h = 1/2, the corresponding transfer diagram of the phase states using Gray and natural mappings is shown in Figure 7.

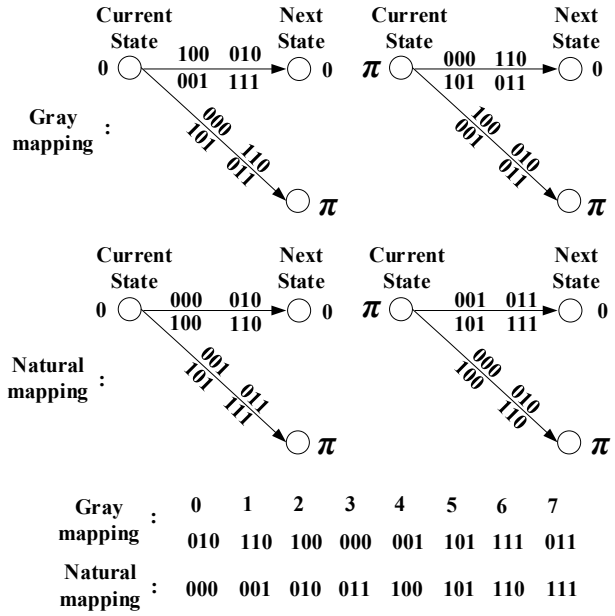

Figure 7. Transfer diagram of the phase states of 8M2RC with h = 1/2 using Gray and natural mappings.

In this case, eight input code symbols and two phase states of 0 and π are presented. Each transfer between the adjacent phase states exists in four possible input code symbols. Information loss in an inappropriate symbol mapping would occur when the MAP-like algorithm in CPM-SISO is used [25], that is:

$$P_I(u^{k,j};O) = H_{u^j} \sum_{u:\ U_k^j = u^j} \mathbf{P}_I(\mathbf{u}^k;O) \prod_{i=1,i\neq j}^{\log_2 M} P_I(u^{k,i},I) \tag{20}$$

With:

$$\mathbf{P}_I(\mathbf{u}^k;O) = H_u\overline{H_u} \sum_{e:\ u(e)=u} A_{k-1}[s^S(e)]\mathbf{P}_I[\mathbf{c}^k;I]B_k[s^E(e)] \tag{21}$$

where H_u, $\overline{H_u}$, and H_{u^j} are normalization constants; $\mathbf{P}_I(\mathbf{c};I)$ is the inner codeword probability of the input; $\mathbf{P}_I(\mathbf{u};I)$ is the inner information probability of the input; $\mathbf{P}_I(\mathbf{u};O)$ denotes the inner information probability of the output; and $A_k(\cdot)$ and $B_k(\cdot)$ are obtained through forward and backward recursions, respectively [28]. On the basis of (20), knowing the identities of the other bits is necessary in deciding on a certain bit. For instance, it is assumed that current and next phase states are 0 and π, separately, there are four possible input code symbols (001, 101, 011, 111) when the natural mapping is used as shown in Figure 7. It is hard to decide whether the first bit is 0 or 1 when the other bits are either 01 or 11. In the Gray mapping case, the decoder can make the appropriate decision on the first bit when the couples of other two mapped bits are different. Consequently, symbol mapping must be chosen carefully for BICM systems with high-order CPM.

NB-LDPC code has many advantages in comparison to binary coding, however, the decoding complexity restricts its development. Since the decoding algorithm of LDPC code is at the symbol level, the decoding complexity will increase rapidly with the increase of Q. In the check-node update of BP decoding, an asymptotical complexity of O (Q^2) for log-decoding or O (Q log2(Q)) for fast fourier transform (FFT) decoding is present. Hence, in comparison to binary coding, the per-bit decoding complexity is (at least) increased by a factor of Q. In practical application, the decoding algorithm can adopt Log-FFT-BP. First, a large number of convolution operations are converted into multiplication operations in frequency domain, and then multiplication operations are converted into addition operations in log domain, which can effectively reduce the decoding complexity.

5. Positive Feedback Issue

For the turbo-like receivers, an unwanted phenomenon called positive feedback, where BER performance worsens with increasing iterations, commonly occurs. A similar phenomenon also occurs in the investigated system, and this is a much more serious phenomenon, especially for low $\mathrm{E_b/N_0}$ due to the insufficient interleaving length and the high possibility of burst errors.

A method of extrinsic information operation is introduced to improve iterative convergence, thereby effectively avoiding the undesired phenomenon. As shown in Figure 1, the extrinsic information from one SISO decoder must be operated and then transmitted into the other SISO decoder, that is:

$$\mathbf{P}_I^*(\mathbf{u}^i, O) = \exp\left(\psi(\mathbf{P}_I(\mathbf{u}^i, O)). \times \ln \mathbf{P}_I(\mathbf{u}^i, O)\right) \tag{22}$$

$$\mathbf{P}_O^*(\mathbf{c}^i, O) = \exp\left(\psi(\mathbf{P}_O(\mathbf{c}^i, O)). \times \ln \mathbf{P}_O(\mathbf{c}^i, O)\right) \tag{23}$$

where $\mathbf{P}_O(\mathbf{c}, O)$ is the outer codeword probability of the output, and $\psi(\cdot)$ is written as:

$$\psi(\mathbf{\Omega}) = a \times \exp(-b|\ln \mathbf{\Omega}|) \tag{24}$$

where a and b are satisfied with $a \in [0.6, 0.9]$ and $b \in [0.001, 0.01]$, respectively.

Figures 8 and 9 show the comparisons between the iterative convergence of the NB-LDPC code for 8M2RC using the proposed method and the original approach when $\mathrm{E_b/N_0}$ is 0.4 and 1.2 dB, where a and b are set to 0.9 and 0.01, respectively. As can be seen from Figure 8, the proposed method can be effectively curbing the positive feedback phenomenon at low $\mathrm{E_b/N_0}$, the value of BER can be reduced approximately by 5×10^{-3} compared with the original method. Figure 9 reveals that the proposed method is capable of accelerating the iterative convergence, improving power efficiency and enhancing the transmission reliability (BER reduce approximately by 2.5×10^{-3} compared with the original method) at medium-high $\mathrm{E_b/N_0}$.

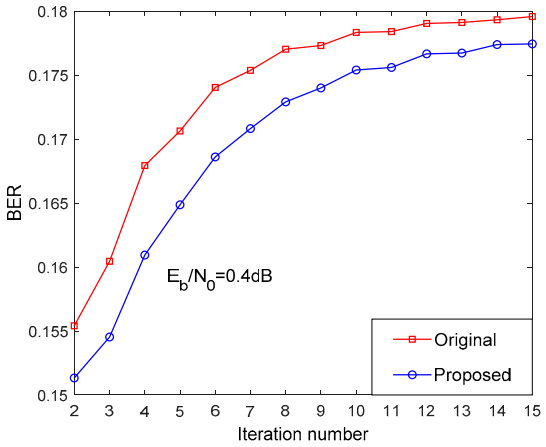

Figure 8. Iterative convergence of the NB-LDPC code for 8M2RC with h = 1/2 using the proposed and original methods at $\mathrm{E_b/N_0} = 0.4$ dB.

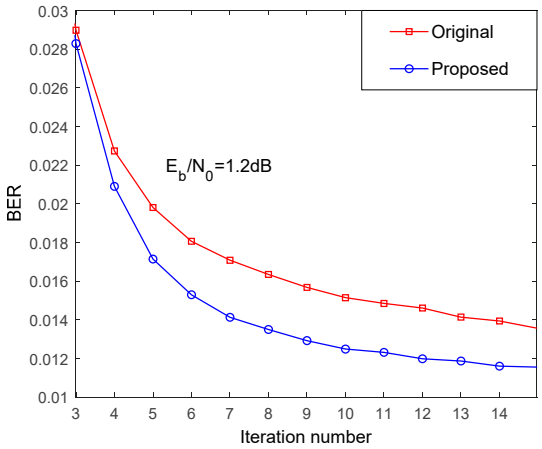

Figure 9. Iterative convergence of the NB-LDPC code for 8*M*2RC with $h = 1/2$ using the proposed and original methods at $E_b/N_0 = 1.2$ dB.

6. Optimization Design for Iterative Efficiency

LDPC decoding is an iterative detector using BP or a modified BP algorithm. Thus, the NB-LDPC-coded CPM systems have two iterative decoding structures at the receiver. The iteration choice has profound effects on iterative decoding performance. However, large numbers of iterations between demodulation and decoding are generally used to achieve excellent BER performance, which adversely increases computational complexity and iterative decoding delay. To improve iterative efficiency, we propose iteration optimization using the EXIT chart and mutual information between demodulation and decoding to achieve the suitable tradeoff for the communication reliability and iterative decoding delay.

The optimized NB-LDPC code for the 8*M*2RC scheme with $\eta = 0.5$ bit/s/Hz and $R = 2/3$ was investigated as an instance. The corresponding EXIT curves of the optimized NB-LDPC code with various inner iterations are shown in Figure 10. Inner iterations have no significant impact on convergence threshold because more iterations barely improve the BER performance at low E_b/N_0.

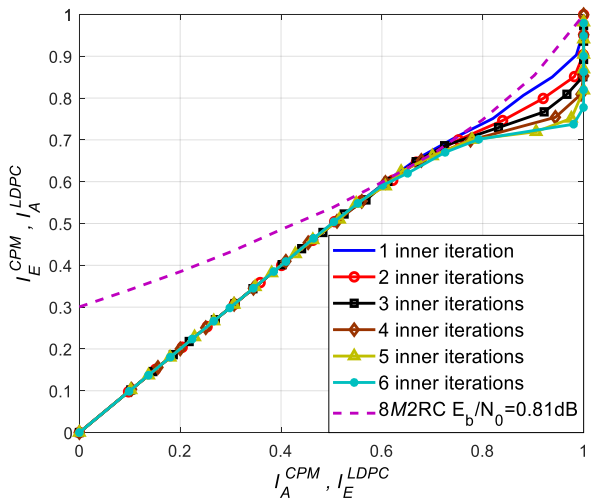

Figure 10. EXIT charts for optimized NB-LDPC code with various inner iterations.

The EXIT curves for NB-LDPC code become steeper with increasing inner iterations, implying a larger iterative space of the CPM-SISO and LDPC-SISO decoder EXIT curves, resulting in an easier convergence with fewer outer iterations. However, the improved trend is no longer evident in five or more inner iterations. Hence, the optimized inner iteration of this design is set to five times.

Once the inner iterations were determined, the optimization of the outer iterations was investigated as follows. Fewer outer iterations are required to achieve a high BER performance with increasing E_b/N_0 in a turbo cliff region. Thus, a limit exists on how to design suitable outer iterations for various E_b/N_0. Mutual information is effective for better understanding the convergence of SISO decoders. A greater amount of mutual information means a more accurate identification of SISO decoders on information symbols. The mutual information of the outer codeword probability of the LDPC-SISO output at the nth iteration is defined as:

$$MI(n) = \log_2 Q - \frac{1}{N}\sum_{i=1}^{N}\sum_{q=0}^{Q-1} P_O^n(c_q^i, O) \times \log_2 \frac{1}{P_O^n(c_q^i, O)} \tag{25}$$

where $P_O^n(c_q^i, O)$ is the probability of an event wherein the ith element in the symbol vector $\mathbf{c}$ equals q. If the difference in mutual information between the current and previous iterations is extremely small, then their BER performance is comparable, and the improved performance is no longer remarkable with the following outer iterations. Therefore, an iterative stopping criterion can be estimated as:

$$MI(n) - MI(n-1) < \varepsilon \tag{26}$$

where ε is an extremely small value (for example, $\varepsilon = 10^{-5}$). If the current iteration satisfies this criterion at a certain E_b/N_0, it is assumed to be the optimal outer iteration, and the next iteration detection is terminated immediately.

7. Simulation Results

In this section, BER simulations for various schemes with $\eta = 0.5$bit/s/Hz and $R = 2/3$ are presented. Figure 11 depicts the BER performance of the optimized NB-LDPC code for 8*M*2RC with various inner iterations at fixed 20 outer iterations. The BER curves using various inner iterations almost coincide within approximately 0.8 dB. This finding indicates that the BER performance at low E_b/N_0 cannot be improved by increasing the iterations again. Conversely, when the E_b/N_0 exceeds the convergence threshold into the turbo cliff region, the BER performance significantly improved as the number of inner iterations increases. However, the improved effect was no longer outstanding after five inner iterations, in perfect agreement with the EXIT chart analysis.

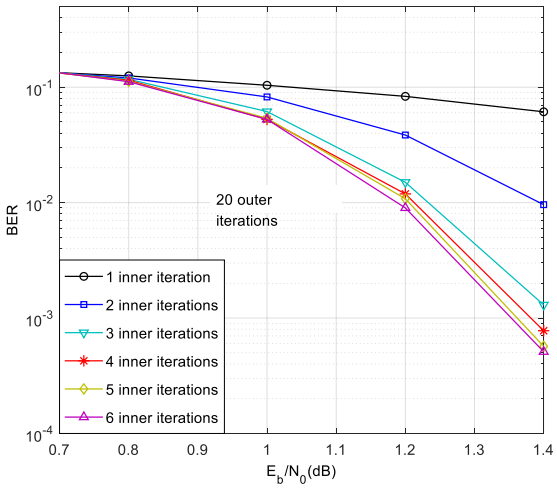

Figure 11. Bit error rate (BER) performance of the optimized NB-LDPC code for 8*M*2RC with various inner iterations.

Figure 12 presents the BER simulations of the resulting scheme (8*M*2RC) and other candidate schemes (8*M*1REC and 4*M*2RC) using the proposed methods for $\eta = 0.5$bit/s/Hz and $R = 2/3$, as well

as their original counterparts with or without extrinsic information operation. In this analysis, a and b were set to 0.9 and 0.01, respectively. To ensure a fair comparison, the VN degree distribution was maintained with that of the resulting scheme.

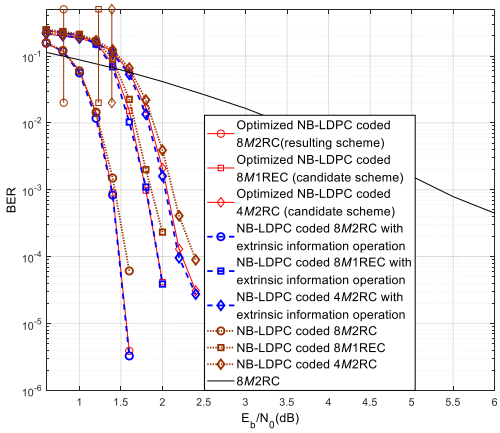

Figure 12. BER performance of the resulting scheme and other candidate schemes for $\eta = 0.5$ bit/s/Hz and $R = 2/3$, as well as their original counterparts with or without extrinsic information operation. The vertical lines represent their convergence thresholds achieved from the EXIT chart. The interleaver length is 1152 symbols.

In Figure 12, the convergence thresholds of all the schemes are reported. The resulting schemes step into the turbo cliff region 0.42 and 0.58 dB earlier and show higher power efficiency compared with 8M1REC and 4M2RC candidate schemes. The resulting scheme provides an approximately 3.95 dB coding gain compared to the uncoded 8M2RC, while achieving approximately 0.5 dB and 0.7 dB advantages over those of 8M1REC and 4M2RC schemes for the BER of 10^{-3}, respectively. The schemes with extrinsic information operation always converge to a smaller BER at the turbo cliff region compared to those without extrinsic information operation and it can achieve approximately 0.1 dB advantages. In addition, Figure 13 shows that these optimized schemes using five inner iterations and $\varepsilon = 1e^{-5}$ have fewer average outer iterations with increasing E_b/N_0 and exhibit negligible BER performance degradation with respect to their original counterparts with a total of 140 iterations (seven inner iterations ×20 outer iterations). These optimized schemes attain a suitable tradeoff of the communication reliability and iterative decoding delay and enhance systematic iterative efficiency.

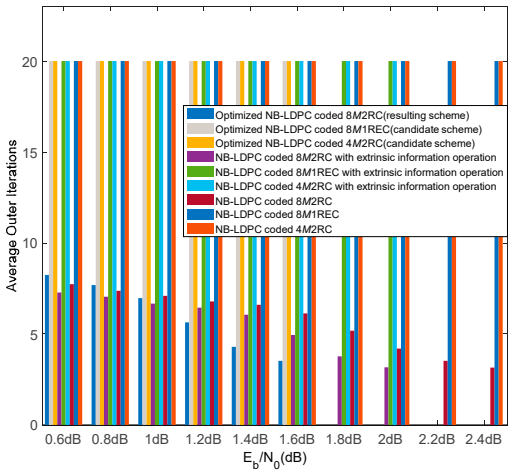

Figure 13. Average outer iteration comparison of the resulting scheme and other candidate schemes for $\eta = 0.5$ bit/s/Hz and $R = 2/3$, as well as their original counterparts with or without extrinsic information operation.

8. Conclusions

The design of the CPM parameter, decoding delay, and the positive feedback problem in iterative decoding are the main factors that limit the development of the coded CPM system. To address the above problems, NB-LDPC-coded high-order CPM systems were designed and optimized in this paper. A novel design method based on the MSNED and $B_{99\%}$ was introduced to explore a competitive CPM scheme using particular η and R under the constraint of implementation complexity. A three-step method based on the EXIT chart and entropy theory was used to design the NB-LDPC code to reduce the convergence threshold, which reduces the convergence threshold by approximately 0.42 and 0.58 dB compared to the candidate schemes. A method of extrinsic information operation was proposed to address the positive feedback phenomenon existing in iterative detection and decoding. The simulation results showed that the proposed method not only effectively inhibits positive feedback phenomenon at low E_b/N_0 but also accelerate iterative convergence at medium–high E_b/N_0, and the value of BER can be reduced by approximately 5×10^{-3}. An improper iteration match between demodulation and decoding was addressed using the EXIT technique and mutual information to improve the iterative efficiency and attain a suitable tradeoff of the communication reliability and the iterative decoding delay. Finally, simulation results show that the resulting NB-LDPC-coded high-order CPM scheme provides an approximately 3.95 dB coding gain compared to the uncoded CPM and achieves approximately 0.5 and 0.7 dB advantages compared with the candidate schemes. The resulting scheme using the proposed method attains the convergence threshold earlier compared with other competitors and further improves power and iterative efficiencies.

Author Contributions: R.X. conceived the idea and established the mathematical modeling. T.W. did the simulations and wrote the paper. Y.S. checked the simulation and analyzed the data. H.T. contributed to the revisions and the discussion of the results. All authors have read and agreed to the published version of the manuscript.

Acknowledgments: This research was supported by the National Natural Science Foundation of China (No. 61873070), the Technology Development Project of the China Research Institute of Radiowave Propagation (No. JW2019-114) and the Heilongjiang Province Key Laboratory of High Accuracy Satellite Navigation and Marine Application Laboratory (No. HKL-2020-Y03).

Conflicts of Interest: The authors declare no conflict of interest.

References

1. Wang, W.; Abeysekera, S.S. Joint data detection and channel estimation for coded and uncoded continuous phase modulation signals. *Wirel. Commun. Mob. Comput.* **2016**, *16*, 223–235. [CrossRef]
2. Qi, J.W.; Makarov, S.B.; Liu, M.X.; Li, B.M.; Xue, W. Research on an Optimization Method for a Partially Responsive Continuous Phase Modulated (CPM) Signal Based on an Optimal Generic Function. *Symmetry* **2019**, *11*, 1114. [CrossRef]
3. Xia, X.; Tang, Z.; Wei, J.; Zhou, Z. Spectrally Efficient Constant Envelope Modulation for GNSS Signals. *Radioengineering* **2018**, *27*, 813–818. [CrossRef]
4. Xue, R.; Sun, Y.B.; Zhao, D.F. CPM Signals for Satellite Navigation in the S and C Bands. *Sensors* **2015**, *15*, 13184–13200. [CrossRef] [PubMed]
5. Xue, R.; Cao, Q.M.; Wei, Q. A Flexible Modulation Scheme Design for C-Band GNSS Signals. *Math. Probl. Eng.* **2015**, *7*, 1–8. [CrossRef]
6. Suffritti, R.; Lombardo, F.; Piemontese, A.; Coralli, A.V. Energy efficient CPM waveforms for satellite mesh networks. In Proceedings of the 2012 IEEE Global Communications Conference, Anaheim, CA, USA, 3–7 December 2012; pp. 3317–3321.
7. Remlein, P. Energy efficient continuous phase modulation signals for satellite intelligent transportation systems. *IET Circuits Devices Syst.* **2014**, *8*, 3255–3259. [CrossRef]
8. Amat, A.G.; Nour, C.A.; Douillard, C. Serially concatenated continuous phase modulation for satellite communications. *IEEE Trans. Wirel. Commun.* **2009**, *8*, 3260–3269. [CrossRef]
9. Xue, R.; Yu, H.; Cheng, Q.L. Adaptive coded modulation based on continuous phase modulation for inter-satellite links of global navigation satellite systems. *IEEE Access* **2018**, *6*, 20652–20662. [CrossRef]

10. Sha, N.; Chen, L.H.; Gao, Y.Y.; Guo, M.X. Serially Concatenated CPM in Two-Way Relay Channels with Physical-Layer Network Coding. *IEICE Trans. Fundam. Electron. Commun. Comput. Sci.* **2019**, *102*, 934–937. [CrossRef]
11. Su, L.B.; Wang, N.Y.; Zhang, Y.N.; Xia, G.J.; Xue, Y.H.; Lv, J.K. Serially concatenated extended CPM scheme based on TDRSS. In Proceedings of the Journal of Physics: Conference Series, Chengdu, China, 13–15 December 2019.
12. Norris, J.A.; Nieto, J.W. Quasi-coherent performance of convolutionally-coded continuous phase modulation. In Proceedings of the SPIE Defense, Security, and Sensing, Baltimore, MD, USA, 28 May 2013.
13. Schuh, F.; Huber, J.B. Nonlinear Trellis Description for Convolutionally Encoded Transmission Over ISI-channels with Applications for CPM. In Proceedings of the 9th International ITG Conference on Systems, Communication and Coding, München, Germany, 21–24 January 2013.
14. Alencar, R.R.M.D.; Landau, L.; Lamare, R.D. Continuous Phase Modulation With 1-Bit Quantization and Oversampling Using Iterative Detection and Decoding. In Proceedings of the Asilomar Conference on Signals, Systems, and Computers, Pacific Grove, CA, USA, 3–6 November 2019.
15. Yan, Q.; Li, Q.; Luo, S.; Li, S.Q. Symbol-Spaced Turbo Frequency Domain Equalization for Precoded Continuous Phase Modulation. *IEICE Trans. Commun.* **2012**, *6*, 2065–2073. [CrossRef]
16. Ngo, H.A.; Maunder, R.G.; Hanzo, L. Extrinsic Information Transfer Charts for Characterizing the Iterative Decoding Convergence of Fully Parallel Turbo Decoders. *IEEE Access* **2017**, *3*, 2100–2110. [CrossRef]
17. Wang, D.D.; Sun, C.H.; Wang, L.Q.; Chen, X. Low complexity multi-level NB-QC-LDPC coded modulation scheme for optical communication systems. In Proceedings of the 17th International Conference on Optical Communications and Networks (ICOCN2018), Zhuhai, China, 16–19 November 2018.
18. Yang, J.C.; Gao, J.P.; Liu, X.L. Code-aided carrier phase synchronization algorithm for non-binary LDPC-CPM system. In Proceedings of the Eleventh International Conference on Graphics and Image Processing (ICGIP 2019), Hangzhou, China, 12–14 October 2019.
19. Benaddi, T.; Poulliat, C.; Boucheret, M.L.; Gadat, B.; Lesthievent, G. Asymptotic analysis and design of LDPC codes for laurent-based optimal and suboptimal CPM receivers. In Proceedings of the 2014 IEEE International Conference on Acoustics, Speech and Signal Processing (ICASSP), Florence, Italy, 4–9 May 2014.
20. Foruhandeh, M.; Uysal, M.; Altunbas, I.; Guven, T.; Gercek, A. Optimal choice of transmission parameters for LDPC-Coded CPM. In Proceedings of the 2014 IEEE Military Communications Conference (MILCOM), Baltimore, MD, USA, 6–8 October 2014.
21. Mostari, L.; Taleb-Ahmed, A. Non-Binary Serial Turbo LDPC Codes Combined with High Order Constellations. *Pertanika J. Sci. Technol.* **2019**, *27*, 33–47.
22. Zhao, D.F.; Sun, Y.B.; Xue, R. Improved iterative convergence method in Q-ary LDPC coded high order PR-CPM. *J. Syst. Eng. Electron.* **2016**, *27*, 541–548. [CrossRef]
23. Xue, R.; Xiao, C.L. Power and Bandwidth Efficient Q-ary LDPC Coded Partial Response Continuous Phase Modulation. In Proceedings of the 2012 8th International Conference on Wireless Communications, Networking and Mobile Computing, Shanghai, China, 21–23 September 2012.
24. Benaddi, T.; Poulliat, C.; Boucheret, M.L.; Gadat, B.; Lesthievent, G. Design of Unstructured and Protograph-Based LDPC Coded Continuous Phase Modulation. In Proceedings of the 2014 IEEE International Symposium on Information Theory, Honolulu, HI, USA, 29 June–4 July 2014.
25. Yu, Z.; Li, Q.Y.; Huang, L.; Dai, K.R.; Song, J. Optimal Design of Cascade LDPC-CPM System Based on Bionic Swarm Optimization Algorithm. *IEEE Trans. Broadcasting* **2018**, *64*, 762–770.
26. Xu, Z.H.; Zhu, J.; Cheng, Q.; Zhang, Z.X. An iterative decoding scheme for CPM-QC-LDPC codes based on matrix transform. *IEICE Trans. Commun.* **2019**, *E102B*, 496–509. [CrossRef]
27. Rimoldi, B.E. A decomposition approach to CPM. *IEEE Trans. Inf. Theory* **1988**, *34*, 260–270. [CrossRef]
28. Bentdetto, S.; Divsalar, D.; Montorsi, G.; Pollara, F. A soft-input soft-output APP module for iterative decoding of concatenated codes. *IEEE Commun. Lett.* **1997**, *1*, 22–24. [CrossRef]
29. Wymeersch, H.; Steendam, H.; Moeneclaey, M. Log-domain decoding of LDPC codes over GF(q). In Proceedings of the 2004 IEEE International Conference on Communications, Paris, France, 20–24 June 2004.
30. Song, H.; Cruz, J.R. Reduced-complexity decoding of Q-ary LDPC codes for magnetic recording. *IEEE Trans. Magn.* **2003**, *39*, 1081–1087. [CrossRef]
31. Arnold, D.; Loeliger, H.A. On the information rate of binary-input channels with memory. In Proceedings of the IEEE International Conference on Communications, Helsinki, Finland, 11–14 June 2001.

32. Pfister, H.D.; Soriaga, J.B.; Siegel, P.H. On the achievable information rates of finite state ISI channels. In Proceedings of the IEEE Global Telecommunications Conference, San Antonio, TX, USA, 25–29 November 2001.
33. Arnold, D.M.; Loeliger, H.A.; Vontobel, P.O.; Kavcic, A.; Zeng, W. Simulation-Based Computation of Information Rates for Channels with Memory. *IEEE Trans. Inf. Theory* **2006**, *52*, 3498–3508. [CrossRef]
34. Padmanabhan, K.; Ranganathan, S.; Sundaravaradhan, S.P.; Collins, O.M. General CPM and its capacity. In Proceedings of the International Symposium on Information Theory, Adelaide, SA, Australia, 4–9 September 2005.
35. Brink, S.T. Convergence of iterative decoding. *Electron. Lett.* **1999**, *35*, 806–808. [CrossRef]
36. Brink, S.T.; Kramer, G.; Ashikhmin, A. Design of low-density parity-check codes for modulation and detection. *IEEE Trans. Commun.* **2004**, *52*, 670–678. [CrossRef]
37. Hu, X.Y.; Eleftheriou, E.; Arnold, D.M. Regular and irregular progressive edge-growth tanner graphs. *IEEE Trans. Inf. Theory* **2005**, *51*, 386–398. [CrossRef]
38. Fan, J.; Xiao, Y. A method of counting the number of cycles in LDPC codes. In Proceedings of the 2006 8th International Conference on Signal Processing, Beijing, China, 16–20 November 2006.